Knocking on surfaces : interactions of hyperthermal particles with metal surfaces

Ueta, H.

Chapter 6

The Interaction of Hyperthermal Nitrogen with N-covered Ag(111)

A mixture of hyperthermal N atoms and N_2 molecules was scattered from the N-covered Ag(111) surface held at 300 K. The angular distribution of scattered N atoms is very broad. In contrast, N_2 molecules exhibit a sharp angular distribution. Taking into account the relative mass ratio, N atoms lose more energy at the surface when compared with N_2. In general N atoms follow the binary collision model, whereas N_2 does not. Instead, the N_2 energy curves are more comparable to the parallel momentum conservation model for outgoing angles of 40°-65°. In both cases the angle-resolved final energy curves are very similar to those from the bare surface. However, the N-covered surface yields non-negligible N_2 intensity for a broad range of outgoing angles, including along the surface normal. This was not the case from the clean surface, where the measured intensity distribution was confined to a much smaller angular range. The possible origin of the N_2 detected at small outgoing angles is considered in terms of backscattering and a direct abstraction reaction. Of these two, an abstraction mechanism appears to be more consistent with the measured data.

6.1 Introduction

In general, due to the strength of the triple bond, N_2 is known as an inert molecule except when adsorbed at the most reactive of surfaces. In this regard the Ag(111) surface is very inert toward N_2 [1, 2]. However, when the molecular bond is broken the resulting N atoms interact strongly with a large range of surfaces. N atom scattering from bare Ag(111) surface has been studied recently [3] and forms chapter 5 of this thesis. The scattered N atoms have a very large angular spread comprised of a broad distribution and a sharp specular peak. The results were interpreted in terms of probing different potential energy surfaces by different electronic states of the N atom. One of these states is very reactive while the other is primarily repulsive in nature.

When an adsorbate is already present on a surface the nature of the surface as seen by incident particles is changed. The extent to which the covered surface differs from the bare surface is dependent on the precise details of the adsorption location and the potential probed by the incident species. Impinging reactive atoms have the added possibility to react with the adsorbate, in addition to sticking and scattering. Previously a number of instances of reactions involving reactive gas with chemisorbed reagents on metal surfaces have been reported. In particular, H atom related reactions have been extensively studied [4-28]. Two primary mechanisms are involve: the *Eley-Rideal* (ER) mechanism in which an adsorbate is abstracted from the surface in a direct collision with an incident atom [29, 30], and the hot atom (HA) mechanism in which incident atoms do not fully accommodated on the surface before they react with an adsorbate and the resulting product desorbs [31]. These mechanisms are non-thermal processes, in contrast to the thermal reaction process—the so-called *Langmuir-Hinschelwood* (LH) mechanism—in which the reagents are chemisorbed and equilibrate at the surface prior to reaction [32, 33]. Even in the absence of a reaction between incident atom and adsorbate, adsorbate desorption may occur as a result of energy released to the adsorbate/lattice if the incoming particle has excess energy (as has been studied in chapter 3) or chemisorbs—the so-called dynamics displacement process [34-37].

In this chapter, hyperthermal N and N_2 interacting with the N-covered Ag(111) surface is described. Previously, recombinative desorption of N_2 from the N-covered Ag(111) surface was studied [2]. It was reported that the angular distribution of the desorbing N_2 had an extremely sharp peak along the surface normal, which could be fitted with a $\cos^{75}\theta_d$ function. Vibrationally and rotationally excited N_2 desorption was inferred from the absence of $N_2(v=0, 1, J)$ states in state-resolved experiments. N adsorption on Ag(111) has been characterised by Wang *et al.* on the basis of DFT calculations [38]. Their calculations of the N adsorption energy as function of adsorption site indicate that the fcc hollow site is the most stable point for adsorption and that the N atoms sit ~1.1-1.4 Å above the Ag atomic plane. Kokh *et al.* computed potential energy curves of ground and excited state N atoms with Ag_{91} clusters using the embedded cluster and multi-reference single- and double-excitation configuration interaction (MRD-CI) methods [39]. They show a large difference between the

potential of ground state $N(^4S)+Ag_{91}$ and excited state $N(^2D)+Ag_{91}$ (see figure 1.4 in this thesis). The $N(^2D)+Ag_{91}$ potential has a more attractive well than the $N(^4S)+Ag_{91}$ potential.

Wang *et al.* have also reported the activation energy for the N_2 dissociation on Cu(111) and Au(111). The barrier heights of N_2 dissociation on Au(111) and Cu(111) are ~6.5 and ~3.75 eV respectively. There have been no similar reports for Ag(111). However, based on the similarity to N atom binding energy on Au(111), N_2 dissociation on Ag(111) can also be expected to have a high activation barrier.

N_2 scattering from the Ag(111) surface has been extensively studied in the incident energy (E_i) range from thermal up to ~1.5 eV [40-42]. For the lower incident energies, N_2 molecules interact with a flat potential energy surface, resulting in the energy distribution of the scattered particles as function of outgoing angle following the parallel momentum conservation model. At the higher incident energy the energy loss is more-or-less constant as a function of outgoing angles, unlike the physisorption system of Ar which qualitatively follows the binary collision. The N_2 angular distribution has a single sharp with peak at around the specular angle. The full width at half-maximum (FWHM) of this peak decreases with increasing incident energy. Those studies indicate that the effective N_2—Ag interaction potential remains relatively flat even at incident energies above 1 eV. Separately, the internal state distribution of scattered N_2 has been investigated in detail [1, 43-47]. N_2 scattering from Ag(111) is different to that from Ru(0001). For Ru(0001), an asymmetrically broadening of the angular distribution with increasing E_i was observed for normal components of E_i of greater than 0.65 eV [48]. This was interpreted in terms of probing a meta-stable molecular chemisorption well.

6.2 Experimental

The experiments have been carried out in a plasma beam scattering apparatus [3, 49, 50]. It consists of a triply differentially-pumped beam line connected to a UHV scattering chamber. The first stage contains the cascaded arc source [51-54]. This source produced a wall-stabilised high-density linear plasma. N_2 (purity 99.999%) plasma is generated by discharge at three symmetrically-mounted cathode tips and is transported through a ∅=2.5 mm channel in a stack of 5 floating, mutually-isolated copper plates before expanding into the first vacuum stage of the beamline. The second stage of the beamline contains a chopper in order to produce a pulsed beam, a beam flag to block the beam, and a pair of deflector plates in order to eliminate charged particles. For time-of-flight (TOF) measurements a double slit 0.5% duty cycle chopper was employed. The third stage functions as a buffer chamber.

The sample is mounted in the centre of the scattering chamber on a three-axis goniometer [55]. A differentially-pumped quadrupole mass spectrometer (QMS) can be rotated around the sample to detect particles leaving from the surface along in-plane scattering directions. In combination with the motion of the manipulator, it is possible to directly measure the incident beam and scattered particle for a large range

of incident angle. By changing the electron impact energy of the QMS ioniser, we detected N at energies below the threshold of the ground state in the direct beam. This confirms that our N beam contained electronically excited N atoms such as N(^{2}D) and N(^{2}P). In contrast, no detectable excited state N_2 was measured.

The Ag crystal used was oriented to within 0.1° of the (111) face. The surface was cleaned by repeated cycles of Ar^+ sputtering follows by annealing to 800 K for several minutes. The surface temperature (T_S) was monitored with a K-type thermocouple inserted into a hole in the side of the crystal. The surface structure was checked by low-energy electron diffraction. N_2 temperature programmed desorption (TPD) spectra from the N-covered Ag(111) surface were in agreement with those reported previously [2]. N-covered surfaces were prepared by continuous (unchopped) beam irradiation at an incident angle (θ_i) of 60° and T_S=300 K.

For the TOF experiments, the flight time of the N and N_2 was measured from the chopper to the rotatable QMS in the scattering chamber. Corrections for a trigger delay and the flight time of ions through the QMS have been applied to the raw data [3, chapter 5]. The incident particle energy, final energies as a function of scattering angle, and angular intensity distributions were all derived from TOF measurements after fitting with shifted Maxwell-Boltzmann (MB) distributions convoluted over the finite chopper opening time and over the spread of arrival times of particles at the surface [49, 56, 57]. In this study, the incident N and N_2 beams had an average energy ($<E_i>$) of ~4.3 eV and ~5.6 eV respectively. Our beams had a broad energy distribution ($E_{FWHM}/<E_i>$~1.14 for N and ~1.13 for N_2).

6.3 Results

6.3.1 N scattering

We begin by focusing on N atom scattering from the N-covered Ag(111) surface. N atoms can stick to the bare surface at room temperature [2]. Figure 6.1(a) shows the angular distribution of N atoms scattered from the N covered surface at T_S=300 K. The incident angle θ_i was 60° with respect to the surface normal. All data points were derived from individual TOF measurements after the corrections for cracking of N_2 and for the instrumental time delays as previously outlined in chapter 5 and [3]. The results for scattering from the bare Ag(111) surface at T_S=500 K are also shown on this panel for comparison. Since adsorbed N atoms undergo recombinative desorption at 500 K [2, 58], this data represents scattering from a quasi-clean surface. The 500 K data has already been discussed in chapter 5 as part of the study on scattering from the clean Ag(111) surface. Qualitatively, the measurements from the two surfaces are very similar. Both N distributions exhibit a sharp peak superimposed on a broad background. The sharp peak is located around the specular angle and its angular position is not influenced by the presence of N to the surface. Note that (in both cases), allowing for out-of-plane scattering with a similar distribution to that of in-plane scattering, the broad background represents the major fraction of scattered N. This

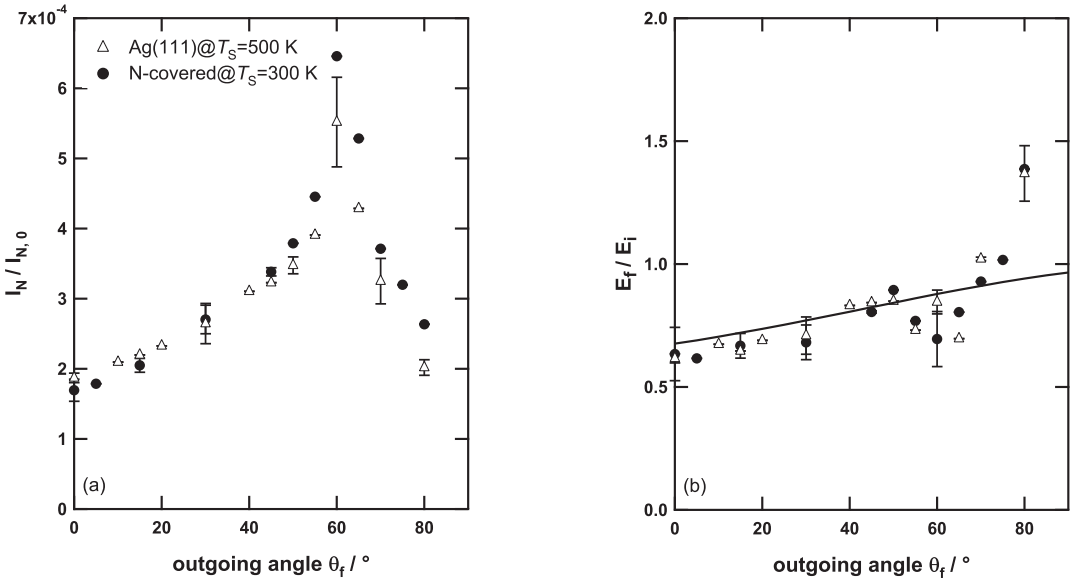

Figure 6. 1 (a) Angular-resolved density distributions of N atoms (<E_i>~4.3 eV) scattered from a bare and N-covered Ag(111) at T_S=500 K and 300 K respectively and at θ_i=60°. The scattered N intensities are normalised to the intensity of the corresponding direct beam. (b) Corresponding angle-resolved ratios of final to initial energy (<E_f>/<E_i>) plotted as a function of the outgoing angle for N atoms scattered from the bare and N-covered surface. The solid line represents the model of single-collision hard-sphere scattering of the incident atoms from an isolated silver atom (mass ratio of m_N/M_{Ag}=14/108). Two independent datasets are plotted for both surfaces.

implies that the majority of scattered N atoms experience an attractive potential energy surface (PES) during their interaction with the surface.

Quantitatively, there are some subtle differences between the two distributions shown on figure 6.1(a). For the N-covered surface: (1) more N atoms are scattered to large outgoing angles; (2) there is more intensity along the specular direction; (3) there appears to be slightly less N scattering to small outgoing angles. The first two points are more evident, whereas the difference at smaller outgoing angles is less pronounced and should be treated with caution.

The corresponding comparison of the angle-resolved N energy ratio (ratio of the average energy after the collision to the average initial energy; <E_f>/<E_i>) is shown in figure 6.1(b). In contrast to the scattered intensity, there does not appear to be any significant change in the energy ratio as a result of N addition to the surface. Any changes that do occur are within the error margins of the determination. The solid line on this panel is the model of a binary collision (hard sphere scattering) of mass 14 (N) with mass 108 (Ag). The data points generally follow or are slightly lower than that model, except at very grazing angle where the average energy of the scattered particles becomes significantly higher than that of the incident beam. Note that since the <E_f> of the scattered N atoms have energies much larger than thermal energy of surface (300 K), there is no indication of any significant thermally trapping at the surface.

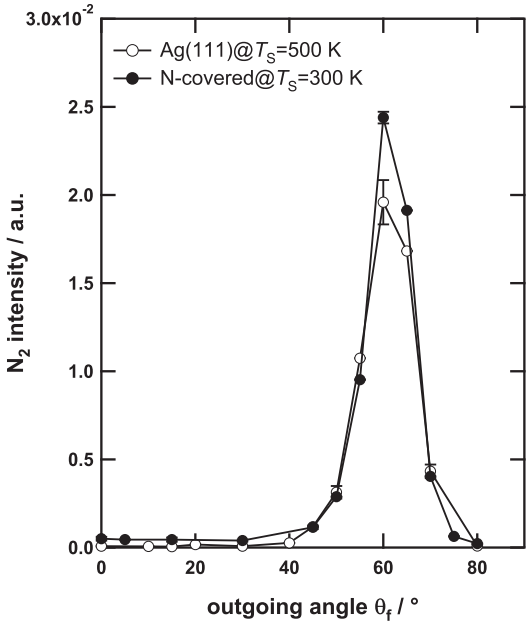

Figure 6. 2 N_2 angular intensity distribution from the bare (T_S=500 K) and N-covered surface (T_S=300 K) at θ_i=60°. These distributions are obtained by integrating the TOF distribution recorded at each outgoing angle. The data has been normalised to the intensity of the corresponding direct beam.

6.3.2 N_2 scattering

As mentioned in the experimental section, our beam contains not only N atoms but also N_2 molecules. Turning our attention to the N_2 scattering, the relevant angular distribution from the N-covered surface (T_S=300 K) is displayed in figure 6.2. This distribution is obtained by integrating the TOF spectra recorded at each outgoing angle in a similar fashion to the procedure used for the N atoms. For comparison purpose, the N_2 angular distribution from clean Ag(111) at T_S=500 K (above the recombinative desorption temperature [2, 58]), is also shown. Both distributions have a sharp peak around the specular angle. The peak intensity for N-covered surface is ~25% larger than that for the clean surface. The FWHM of the N_2 distribution from the clean and N-covered surfaces are ~13° and ~11° respectively. Note that the FWHM values for this beam energy are comparable to the previous result (~14°) obtained for E_i=1.5 eV under similar experimental conditions (T_S=600 K and θ_i=60°) [42].

The main difference between the two distributions is that N_2 signal was detectable in the TOF spectra at *all* outgoing angles measured from the N-covered surface, including along the surface normal. This results in the low intensity broad component that is evident in figure 6.2. In contrast, no scattered N_2 was detectable at small outgoing angle (θ_f<40°) in the measurements from the clean surface.

Figure 6.3 shows a series of N_2 TOF spectra collected from the N-covered surface at T_S=300 K. In this figure a single shifted MB distribution has been fitted to all spectra under the assumption that the distributions are solely the result of scattering of N_2. It is evident that the spectra cannot be well-described by such a distribution, in particular for the outgoing angles between 55° and 70°. The fits of a single distribution to the spectra in this region are very poor. The fits to the TOF spectra

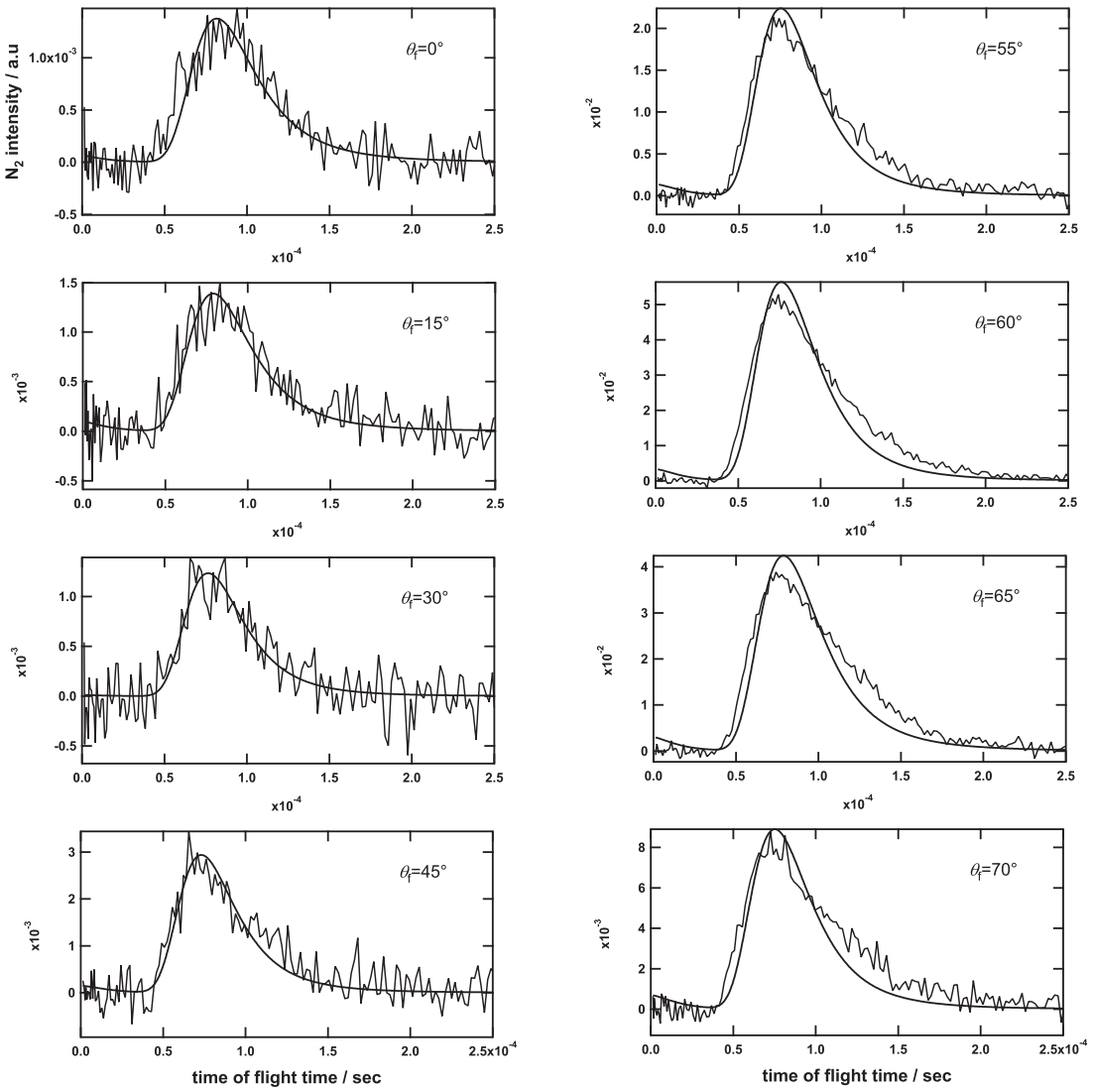

Figure 6. 3 A series of N_2 TOF spectra collected from the N-covered surface at T_S=300 K at different θ_f (θ_i=60°). The fitted curves are based on the assumption of a single shifted Maxwell-Boltzmann distribution arising from scattering of N_2.

measured at small outgoing angles are better, but still not entirely satisfactory. The angle-resolved $<E_f>/<E_i>$ curve derived from the fittings shown in figure 6.3 is plotted in figure 6.4. It qualitatively follows the binary collision model for small outgoing angles, but the calculated energy ratio drops dramatically around the specular region. Note that the poor description of the TOF spectra around the specular direction by a singled shifted MB distribution is equally the case for the measurements from the clean surface (not shown). This is a feature of measurements that is independent of the presence of adsorbed N.

Alternative fitting results on the basis of two components (two independent shifted MB distributions, both assumed to originate from incident N_2) are shown in figure 6.5. The fit requires six parameters as described in chapter 2 and [59]. This approach makes it very easy to obtain a good description of the overall shapes of the TOF distributions at all outgoing angles. The derived angle-resolved $<E_f>/<E_i>$ ratios for the individual components and for the overall distribution are shown in figure 6.6. The energy of the slow component is almost constant as function of outgoing angle within

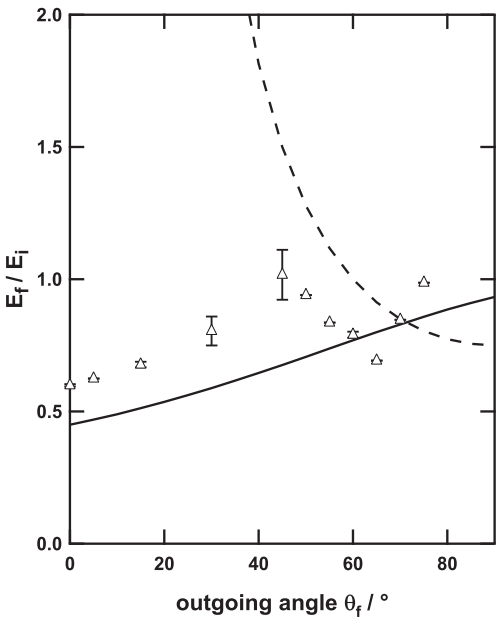

Figure 6. 4 Angle-resolved ratios of final to initial energy ($\langle E_f \rangle / \langle E_i \rangle$) plotted as a function of θ_f for N_2 spectra acquired from the N-covered surface. The values were derived from a single shifted Maxwell-Boltzmann distribution the fittings assuming scattering of incident N_2, which are illustrated on figure 6.3. The solid line represents the model of single-collision hard-sphere scattering of the incident atoms from an isolated silver atom (mass ratio of m_{N_2}/M_{Ag}=28/108). The dashed line corresponds to parallel momentum conservation.

the accuracy of the determination. In contrast, the energy of the fast component undergoes large variations, and there is a net energy gain at small outgoing angles. The final energy determined under the assumptions employed is remarkably high at those angles. The values of that overall average energy follow the trend set by the fast component. It should be noted that since our detector is density sensitive, the apparent fast component in a TOF spectrum appears smaller than it actually is in flux-corrected terms. Thus the contribution from the fastest particles—which were not well described by the single shifted MB fitting—has a significant effect on the value of average energy. As is evident from figure 6.6, the trends and absolute values determined within the θ_f=40°-70° region from the N-covered surface are indistinguishable from those of the bare Ag(111) surface at T_S=500 K.

6.4 Discussion

6.4.1 N scattering

As outlined in the previous section, some minor changes are observed in the angular distribution upon adsorption of N, whereas the energy distributions appear unchanged within the margin of error. Since a lower surface temperature is required to adsorb N, the changes that are observed may be due to the presence of N atoms in the threefold hollow sites, but can also be related to the relative differences in the thermal motion of the surface atoms, or to a combination of both effects. In any case, the very broad

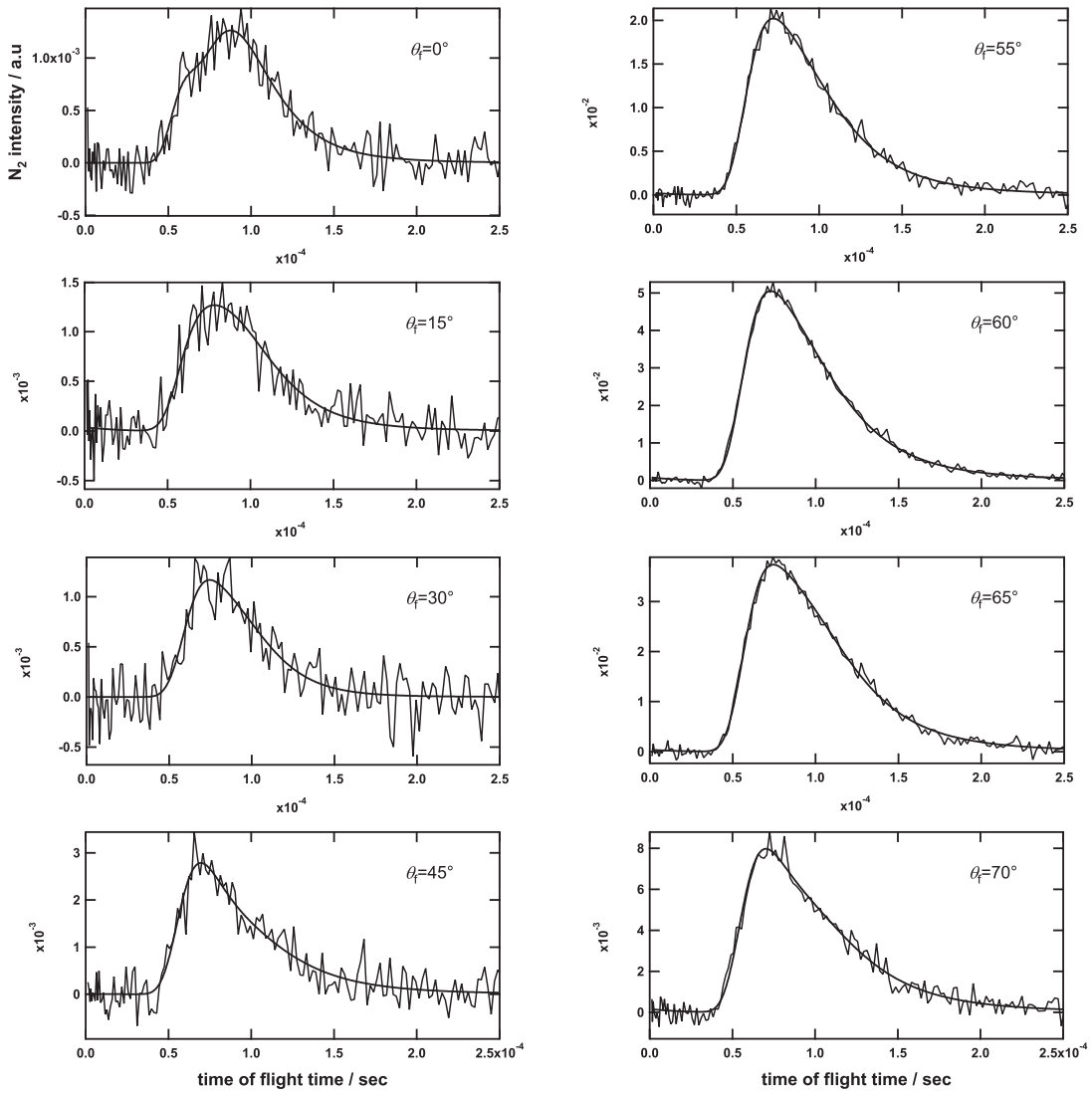

Figure 6. 5 The series of N_2 TOF spectra collected from the N-covered surface at T_S=300 K (same TOF spectra as shown in figure 6.3). These spectra have been fitted with two shifted MB distributions under the assumption that both originate from scattering of incident N_2.

angular distribution strongly suggests that the surface potential "seen" by the majority of incident N atoms remains a deep attractive well.

The deep potential well remains present, as was the case for the NO+H-Ru(0001) system. For that system adsorbed H induces a very local change of the surface potential in the unit cell (fcc-threefold hollow site) that leads to a very sharp angular distribution of scattered NO by passivation [60]. However, the sticking coefficient for NO remained high, suggesting that the attractive potential remained present in another part of the unit cell (hcp-threefold hollow site).

The minor changes observed for the present system suggests that both threefold hollow sites remain attractive to incident N atoms. In chapter 5, N scattering from Ag(111) was interpreted in terms of the probing of different potentials by different electronic state of N atom [3]. As shown in figure 6.1, results from the N-covered surface are similar to those from the clean surface. Thus adsorbed N does not

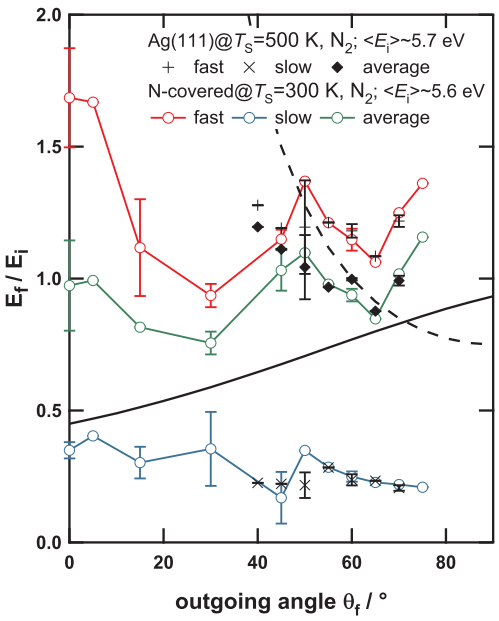

Figure 6. 6 Angle-resolved ratios of final to initial energy (<E_f>/<E_i>) plotted as a function of θ_f for N_2 scattering from the N-covered surface. These values were derived from the fitting with two shifted MB distributions shown in figure 6.5. The solid line represents the model of single-collision hard-sphere scattering of the incident atoms from an isolated silver atom (mass ratio of m_{N_2}/M_{Ag}=28/108). The dashed line corresponds to parallel momentum conservation. For comparison purpose, those equivalent results for fitting to spectra acquired from the bare surface are also plotted.

significantly affect the surface potential for the different states of the N atom. Subtle effects induced by adsorbed N, such as for instance an enhanced repulsive corrugation, are largely invisible to the incident N atoms.

6.4.2 N_2 scattering

The N_2 angular distributions from clean and N-covered surface are very sharp. This indicates an interaction with an uncorrugated repulsive potential and that both surfaces appear structurally smooth to the incident particles. The near-specular peak is slightly sharper and more intense in the case of the N-covered surface. The angle-resolved <E_f>/<E_i> curves at θ_f=40°-70° are almost identical. Neither show an increase in <E_f>/<E_i> with increasing angle θ_f as was observed for Ar scattering from Ag(111) at θ_f=30°-80° [3, chapter 5]. Both the clean and N-covered surface show a very small energy loss for N_2 scattered around the specular direction. This indicates that the N adsorbates do not dramatically modify the effective surface for incident N_2.

The adsorbed N might not be visible to the incident molecules, since the threefold hollow adsorption site allows it to sit relatively deep in the surface layer (binding position is ~1.1-1.4 Å above the Ag atomic plane [38]). For Ar—Ag(111) potentials, Ar with E_i=3 eV could only approach to within about 2 Å of the surface Ag atom cores for the Ag(111) surface [61]. This suggests that the repulsive potential seen by the incident N_2 is largely unchanged by the presence of N-atoms, because they are too

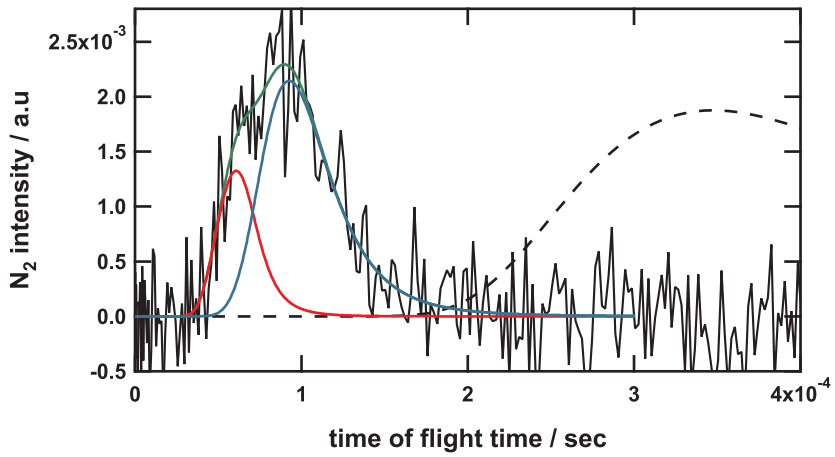

Figure 6. 7 N_2 TOF spectrum for θ_f=0° compared with a simulated 300 K MB distribution, which assumes incident N_2 trapping on the surface followed by thermal desorption (dashed line). In addition, the results of fitting the TOF spectrum with two shifted MB distributions assuming the incident N atom-induced N_2 desorption are illustrated.

deeply adsorbed. Only the incident particles with the highest initial energy would be able to probe sufficiently deep into the surface to directly interact with the adsorbed atoms.

In the case of scattering from the N-covered surface, there is a non-negligible N_2 intensity present at small outgoing angles, as shown in figure 6.2. Figure 6.7 shows the N_2 TOF spectrum for θ_f=0°compared with a simulated 300 K MB distribution, which assumes incident N_2 trapping on the surface followed by thermal desorption. It is obvious that the measured N_2 intensity cannot be attributed to a thermally desorbing component. In addition, since the experiments on the N-covered surface were performed at T_S=300 K, thermal recombinative desorption should not occur. Figure 6.7 also illustrates the result of fitting the TOF spectrum with two shifted MB distributions assuming the incident particle is an N atom.

One possible explanation for the additional N_2 signal that appears when N is present on the surface is related to surface roughness. As already discussed the N atoms reside in the threefold hollow sites of the surface. In the case of Ru it is known that this leads to small local displacements of the surface atoms. These local relaxations might give rise to a loss of long range order. Adsorbing N atoms on the Ag(111) surface have been reported to results in a disordered structure at 300 K based on LEED [2]. Hence, the surface might consist of small patches of well ordered (and atom reflecting) domains separated by steps. In such a case the resulting scattering pattern would be the sum of the scattering from the ordered, flat domains and from the highly corrugated stepped regions. A stepped and corrugated surface region could lead to N_2 backscattering to small outgoing angles. N_2 with thermal energy scattering from the well-defined corrugated Cu(110) surface of exhibits only broad scattering around the specular in-plane, whereas diffraction like features were observed out-of-plane [62]. Note that there is a more or less symmetric broadening of the distribution

in such a case. Thus if scattering at steps is relevant, one would expect a uniform broadening of the angular distribution on both sides of the specular peaks.

In the present case, the very high and sharp N_2 specular peak is evidence that scattering from well-ordered domains dominates on both the clean and N-covered surfaces. If steps lead to the additional broad feature for scattering from the N-covered, then they represent only a small fraction of the total surface. There is indeed some additional N_2 intensity at θ_f=80° for N-covered surface. However, the intensity gain at θ_f=80° is much less than the increase at small outgoing angles. For the N-atom distributions (figure 6.1(a)) the situation was reversed. In that case there an increase in the intensity at large θ_f but the intensity at small θ_f was unchanged or even slightly reduced. These trends suggest that the N_2 signal at small θ_f is not the result of scattering from randomly distributed steps.

Considering the two component fittings shown in figure 6.6—necessary for a proper description at all θ_f—there is no obvious explanation for the large energy gain at small outgoing angles if the fast N_2 component does indeed arise from scattering. This also suggests that the N_2 signal around the normal cannot be due to N_2 scattering. Note however that when a single component fitting is considered the $<E_f>/<E_i>$ values and trend at small outgoing angle are quite reasonable from a mechanical scattering perspective. As illustrated in figure 6.3, single MB fits to the individual TOF distributions are relatively acceptable for these outgoing angles, as compared with similar fits for the near-specular angles.

An alternative to a scattering process is that a direct ER abstraction or HA reaction creates the small additional N_2 intensity across a broad range of outgoing angles. In this case, the molecules detected would be associated with the incident N atoms rather than the incident N_2. This alters the basis on which intensity and energy values are derived from fitting the TOF distributions. Figure 6.8 shows final energies and beam-normalised intensities derived from the TOF distributions measured for θ_f=0°-45° for the two different two component fitting scenarios. The first set (figure 6.8(a) and (b)) assumes that both N_2 components along these outgoing angles arise from recombination involving incident N atoms. The second set (figure 6.8(c) and (d)) assumes that both arise from scattering of incident N_2 molecules. The data in the latter case is the same as that shown in figure 6.6, except that $<E_f>$ is plotted instead of $<E_f>/<E_i>$.

It should be noted that, similar to N_2 scattering scenario, the spectra for θ_f=0°-40° can be also be fitted reasonable well with a single MB under the assumption of N-induced N_2 formation. The quality of this fit is comparable to that shown in figure 6.3 and the trend in E_f derived is similar to that shown on figure 6.4, although the absolute values are lower. This is a general feature: fitting analysis based on using the spread of arrival times of incident N_2 molecules always results in a higher E_f than when based on the arrival times of N, since the incident N_2 is slower than the incident N. Note that there is no indication that ER/HA type reactions are having a significant contribution to the N_2 measured for θ_f=40°-70°. The TOF distributions at these angles

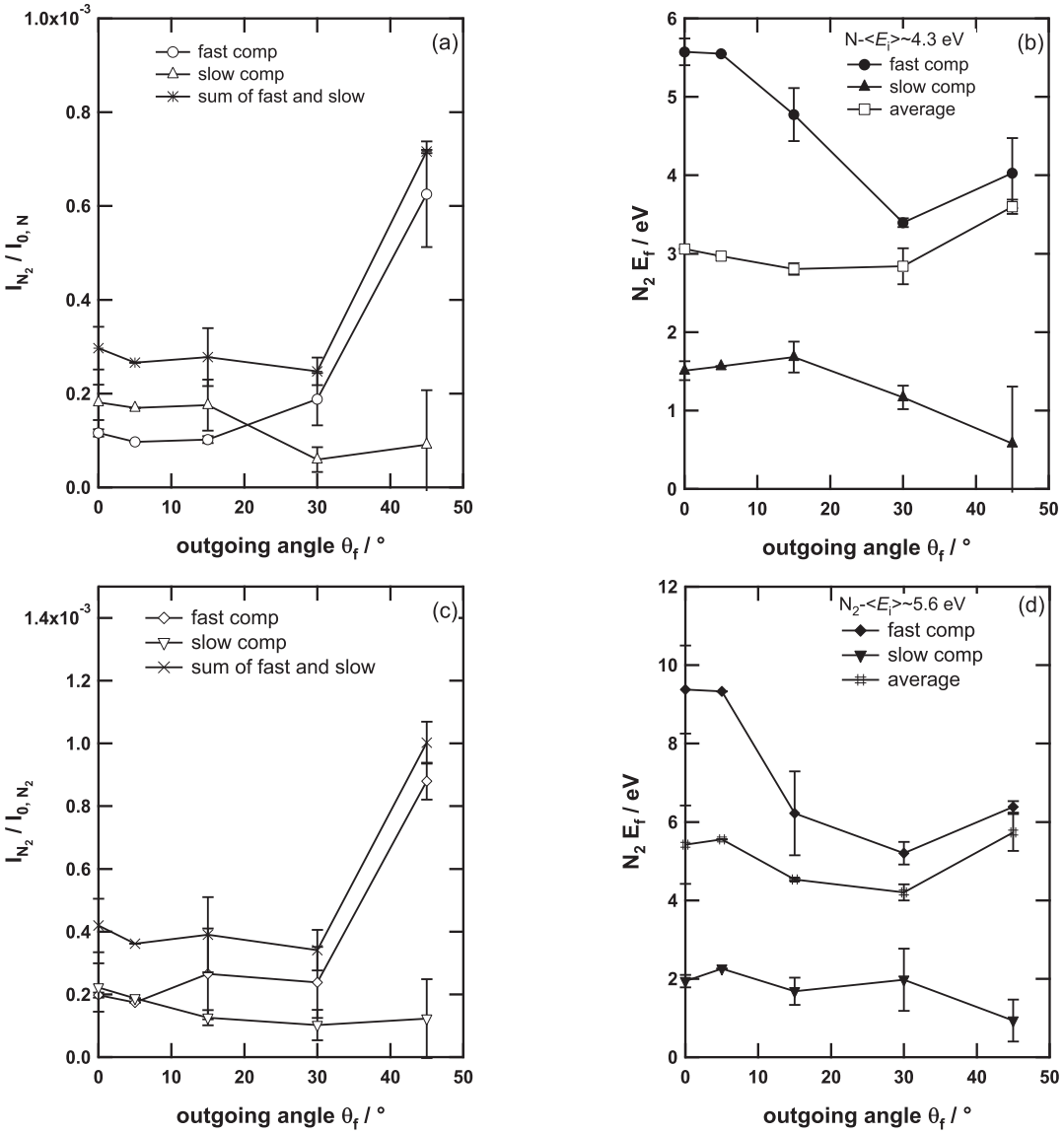

Figure 6. 8 Intensity and energy distribution of two component fitting determined from fittings of the N_2 TOF distributions measured for θ_f=0°-45°. N_2 angular-resolved (a) intensity and (b) energy distributions that were derived based on the assumption that both N_2 components along these outgoing angles arise from recombination reactions involving incident N atoms. (c) and (d) were derived based on the assumption that both arise from scattering of incident N_2 molecules.

are directly comparable to those from the clean surface, where no reaction pathway is available.

As illustrated in figure 6.7, two component MB fitting invariably produced a better match to overall TOF spectra than a single component fitting. This is the case, irrespective of the parent particle that is considered. There are several reasons why N-induced N_2 might indeed exhibit two components. These include:

- The presence of more than one excitation state of N in the incident beam as confirmed by appearance potential measurement;

- The possibility that the two reaction pathway (ER and HA) may by simultaneously operative and producing significantly different N_2 energy distributions.

Comparing the two fitting scenarios shown in figure 6.8, the trends in the angular intensities of the individual components are not significantly affected by the choice of originating particle, although the relative contribution does changes slightly. The trends in the angular energies are also independent of the chosen parent. However, the absolute final energies do change dramatically. As mentioned above, it is difficult to account for the high energy of the fast component derived under the assumption of N_2 scattering. In contrast, it is easier to account for the energy that is predicted if recombination of an incident N and an adsorbed N atom gives rise to fast N_2. The N≡N bond energy is ~9.8 eV. The adsorption energy of a N atom on Ag(111) is about 4 eV, which is the upper limit of reported values based on DFT calculations, with the N atoms binding in hollow sites [38]. In the extreme case of direct ER for recombination of a gas phase N atom and an adsorbed N on Ag(111) is exothermic by ~5.8 eV. Separately, the scattered N atoms can retain a substantial fraction of their original energy, even at small outgoing angles as shown in figure 6.1(b). N_2 produced as a result of ER can be expected to carry a significant amount of excess energy, not only in translation but also in ro-vibrationally excitation. Carter *et al.* showed extremely sharp angular distributions for desorbing N_2 from N-Ag(111) [2]. The N_2 signal that may arise from atom recombination in the current measurements has a much broader angular distribution, as is clear from figure 6.2. This can be attributed to incident translational energy of the N-atoms which is in part retained production of N_2, particular if an ER process is occurring.

Note that if N atom related ER recombinative desorption does occur one can envisage that the reaction cross-section will be small since the adsorbed N atoms are relatively close the surface (the hollow site binding position is ~1.1-1.4 Å above the Ag atomic plane [38]). Steering effects will not be strong due to the hyperthermal energy of the incident atoms, unlike in previous reported instances of pick-up reactions on H+H/metal and H+Cl/metal surfaces [27, 28]. Hence, for a recombinative reaction to be effective, the trajectory of the incident N would be required to pass very close to the adsorbed atom on the surface. As such, the mechanism may be restricted to the high energy fraction of the incident N distribution, since only these atoms have sufficient energy to approach close to the adsorbed atoms. Alternatively, as evident from the very broad N angular distribution (see figure 6.1(a)), the majority of N atoms experience an attractive interaction with the surface, while retaining relatively high translational energy. Multiple collisions at very corrugated PES can be anticipated. Thus, recombinative desorption as a result of a HA reaction mechanism is also feasible.

At present, it is impossible to definitively conclude whether the N_2 signal at small θ_d is due to (in-)elastically scattered N_2 or to an abstraction reaction processes involving incident N. However, the ER/HA based explanation appears to be more

consistent with the measured data. Additional experiments (e.g. using isotopically labelled N_2) and theoretical analysis will be required for a full confirmation.

6.5 Conclusions

Hyperthermal N atoms and N_2 molecules were scattered from the N-covered Ag(111) surface held at 300 K. The results of N atoms and N_2 molecules are similar to those from clean surface. The main difference is the presence of N_2 intensity around the surface normal. In general adsorbed N does not significantly affect the surface potential for N atoms and N_2 molecules. The enhanced intensity around the specular direction suggests that the 300 K N-covered surface appears slightly smoother than the 500 K clean surface. The N_2 desorption around the surface normal may be the result of incident N atom recombination with adsorbed N leading to N_2 desorption.

Bibliography

[1] A.C. Kummel, G.O. Sitz, R.N. Zare, J.C. Tully, The Journal of Chemical Physics, **91** (1989) 5793-5801.
[2] R.N. Carter, M.J. Murphy, A. Hodgson, Surface Science, **387** (1997) 102-111.
[3] H. Ueta, M.A. Gleeson, A.W. Kleyn, The Journal of Physical Chemistry A, **113** (2009) 15092-15099.
[4] P.J. Eenshuistra, J.H.M. Bonnie, J. Los, H.J. Hopman, Physical Review Letters, **60** (1988) 341.
[5] E.W. Kuipers, A. Vardi, A. Danon, A. Amirav, Physical Review Letters, **66** (1991) 116.
[6] E.W. Kuipers, A. Vardi, A. Danon, A. Amirav, Surface Science, **261** (1992) 299-312.
[7] C.T. Rettner, Physical Review Letters, **69** (1992) 383.
[8] B. Jackson, M. Persson, Surface Science, **270** (1992) 195-200.
[9] C.T. Rettner, D.J. Auerbach, Science, **263** (1994) 365-367.
[10] C.T. Rettner, The Journal of Chemical Physics, **101** (1994) 1529-1546.
[11] C.T. Rettner, D.J. Auerbach, Physical Review Letters, **74** (1995) 4551.
[12] C.T. Rettner, D.J. Auerbach, Surface Science, **357-358** (1996) 602-608.
[13] C.T. Rettner, D.J. Auerbach, J. Lee, The Journal of Chemical Physics, **105** (1996) 10115-10122.
[14] M.E. Castro, R.B. Hall, C.A. Mims, The Journal of Physical Chemistry B, **101** (1997) 8048-8051.
[15] S. Caratzoulas, B. Jackson, M. Persson, The Journal of Chemical Physics, **107** (1997) 6420-6431.
[16] S. Wehner, J. Kuppers, The Journal of Chemical Physics, **109** (1998) 294-300.
[17] D.V. Shalashilin, B. Jackson, The Journal of Chemical Physics, **109** (1998) 2856-2864.
[18] J.-Y. Kim, J. Lee, Physical Review Letters, **82** (1999) 1325.
[19] D.V. Shalashilin, B. Jackson, M. Persson, Faraday Discussions, **110** (1998) 287-300.
[20] C. Kalyanaraman, D. Lemoine, B. Jackson, Physical Chemistry Chemical Physics, **1** (1999) 1351-1358.

[21] M. Persson, J. Stromquist, L. Bengtsson, B. Jackson, D.V. Shalashilin, B. Hammer, The Journal of Chemical Physics, **110** (1999) 2240-2249.
[22] D.V. Shalashilin, B. Jackson, M. Persson, The Journal of Chemical Physics, **110** (1999) 11038-11046.
[23] J.-Y. Kim, J. Lee, The Journal of Chemical Physics, **112** (2000) 6015-6022.
[24] J.-Y. Kim, J. Lee, The Journal of Chemical Physics, **113** (2000) 2856-2865.
[25] B. Jackson, D. Lemoine, The Journal of Chemical Physics, **114** (2001) 474-482.
[26] J. Biener, E. Lang, C. Lutterloh, J. Kuppers, The Journal of Chemical Physics, **116** (2002) 3063-3074.
[27] D. Lemoine, J.G. Quattrucci, B. Jackson, Physical Review Letters, **89** (2002) 268302.
[28] J.G. Quattrucci, B. Jackson, D. Lemoine, The Journal of Chemical Physics, **118** (2003) 2357-2366.
[29] D.D. Eley, E.K. Rideal, Nature (London), **146** (1940) 40.
[30] D.D. Eley, Proceedings of the Royal Society of London. Series A. Mathematical and Physical Sciences, **178** (1941) 452-464.
[31] J. Harris, B. Kasemo, Surface Science, **105** (1981) L281-L287.
[32] I. Langmuir, Transactions of the Faraday Society, **17** (1922) 621-654.
[33] C.N. Hinshelwood, Ann. Res. London Chem. Soc, **27** (1930) 11.
[34] C.T. Rettner, J. Lee, The Journal of Chemical Physics, **101** (1994) 10185-10188.
[35] C.T. Rettner, D.J. Auerbach, The Journal of Chemical Physics, **105** (1996) 8842-8848.
[36] C. Åkerlund, I. Zoric, B. Kasemo, Surface Science, **418** (1998) 543-554.
[37] L. Diekhöner, H. Mortensen, C. Akerlund, A. Baurichter, A.C. Luntz, The Journal of Chemical Physics, **114** (2001) 4215-4220.
[38] G.C. Wang, L. Jiang, X.Y. Pang, J. Nakamura, The Journal of Physical Chemistry B, **109** (2005) 17943-17950.
[39] D.B. Kokh, R.J. Buenker, J.L. Whitten, Surface Science, **600** (2006) 5104-5113.
[40] H. Asada, Japanese Journal of Applied Physics, **20** (1981) 527-536.
[41] H. Asada, T. Matsui, Japanese Journal of Applied Physics, **21** (1982) 259-263.
[42] A. Raukema, R.J. Dirksen, A.W. Kleyn, The Journal of Chemical Physics, **103** (1995) 6217-6231.
[43] A.C. Kummel, G.O. Sitz, R.N. Zare, J.C. Tully, The Journal of Chemical Physics, **89** (1988) 6947-6955.
[44] G.O. Sitz, A.C. Kummel, R.N. Zare, Journal of Vacuum Science & Technology A: Vacuum, Surfaces, and Films, **5** (1987) 513-517.
[45] G.O. Sitz, A.C. Kummel, R.N. Zare, The Journal of Chemical Physics, **87** (1987) 3247-3249.
[46] G.O. Sitz, A.C. Kummel, R.N. Zare, The Journal of Chemical Physics, **89** (1988) 2558-2571.
[47] G.O. Sitz, A.C. Kummel, R.N. Zare, J.C. Tully, The Journal of Chemical Physics, **89** (1988) 2572-2582.
[48] D.C. Papageorgopoulos, B. Berenbak, M. Verwoest, B. Riedmüller, S. Stolte, A.W. Kleyn, Chemical Physics Letters, **305** (1999) 401-407.
[49] A. Raukema, Dynamics of Chemisorption, in, University of Amsterdam, 1995.
[50] F. Gou, M.A. Gleeson, J. Villette, A.W. Kleyn, Vacuum, **81** (2006) 196-201.
[51] M.C.M. van de Sanden, G.M. Janssen, J.M. de Regt, D.C. Schram, J.A.M. van der Mullen, B. van der Sijde, Review of Scientific Instruments, **63** (1992) 3369-3377.
[52] R.P. Dahiya, M.J. de Graaf, R.J. Severens, H. Swelsen, M.C.M. van de Sanden, D.C. Schram, Phys Plasmas, **1** (1994) 2086-2095.

[53] M.C.M. van de Sanden, R.J. Severens, J.W.A.M. Gielen, R.M.J. Paffen, D.C. Schram, Plasma Sources Sci T, **5** (1996) 268-274.
[54] S. Mazouffre, I. Bakker, P. Vankan, R. Engeln, D.C. Schram, Plasma Sources Science and Technology, **11** (2002) 439.
[55] A. Raukema, A.P. de Jongh, H.P. Alberda, R. Boddenberg, F.G. Giskes, E. de Haas, A.W. Kleyn, H. Neerings, R. Schaafsma, H. Veerman, Meas Sci Technol, **8** (1997) 253-261.
[56] K.C. Janda, J.E. Hurst, C.A. Becker, J.P. Cowin, D.J. Auerbach, L. Wharton, The Journal of Chemical Physics, **72** (1980) 2403-2410.
[57] M.E.M. Spruit, E.W. Kuipers, F.H. Geuzebroek, A.W. Kleyn, Surface Science, **215** (1989) 421-436.
[58] S.K. So, R. Franchy, W. Ho, The Journal of Chemical Physics, **91** (1989) 5701-5706.
[59] H. Ueta, M.A. Gleeson, A.W. Kleyn, accepted by The Journal of Chemical Physics.
[60] D.A. Butler, B. Berenbak, S. Stolte, A.W. Kleyn, Physical Review Letters, **78** (1997) 4653-4656.
[61] R.J.W.E. Lahaye, A.W. Kleyn, S. Stolte, S. Holloway, Surface Science, **338** (1995) 169-182.
[62] K.H. Rieder, W. Stocker, Physical Review B, **31** (1985) 3392.